Bull. Mater. Sci. (2018) 41:50
https://doi.org/10.1007/s12034-018-1568-4

Green synthesis of zinc oxide nanoparticles using aqueous extract of *Garcinia mangostana* fruit pericarp and their photocatalytic activity

MOHAMMOD AMINUZZAMAN[1,*], LIM POH YING[1], WEE-SHENOG GOH[1] and AKIRA WATANABE[2]

[1]Department of Chemical Science, Faculty of Science, Universiti Tunku Abdul Rahman (UTAR), Perak Campus, Jalan Universiti, Bandar Barat, 31900 Kampar, Malaysia

[2]Institute of Multidisciplinary Research for Advanced Materials (IMRAM), Tohoku University, Katahira 2-1-1, Aoba-ku, Sendai 980-8577, Japan

*Author for correspondence (mohammoda@utar.edu.my)

MS received 16 June 2017; accepted 15 August 2017; published online 29 March 2018

Abstract. We reported a facile, green and eco-friendly approach for the synthesis of zinc oxide nanoparticles (ZnO NPs) using aqueous extract of *Garcinia mangostana* (*G. mangostana*) fruit pericarp as reducing agent as well as capping agent. Biosynthesized ZnO NPs were characterized by various analytical tools using X-ray diffraction, Fourier transform infrared spectroscopy, field emission scanning electron microscopy, transmission electron microscopy, energy dispersive X-ray spectroscopy and UV–Vis spectroscopy. The results showed that ZnO NPs synthesized by aqueous extract of *G. mangostana* fruit pericarp with high purity, mostly spherical in shape with an average size of 21 nm. The photocatalytic activity of biosynthesized ZnO NPs was evaluated by carrying out the degradation of malachite green dye under solar irradiation. The extent of MG dye degradation was monitored spectrophotometrically by measuring absorbance at its characteristics λ_{max} value of 615 nm. Degradation products were detected using liquid chromatography–mass spectrophotometry technique. The biosynthesized ZnO NPs showed an excellent photocatalyst performance due to the small size and high purity.

Keywords. Green synthesis; ZnO nanoparticles; photocatalyst; dye; photodegradation.

1. Introduction

The discharge of dye effluents from various industries such as dye stuffs, textiles, paint and varnishes, inks, plastics, pulp and paper, food, rubber, and cosmetics to the environment is a prime cause of concern nowadays [1]. The effluents from these industries cause the water bodies not only to become coloured, but also lead to a reduction in sunlight penetration, decreasing photosynthetic activity, dissolved oxygen concentration and water quality; and having acute toxic effects on aquatic plants, causing severe environmental problems worldwide [2]. In addition, many synthetic dyes and their metabolites are toxic, mutagenic and carcinogenic [3]. Hence, it is necessary and vital to treat the dye effluents prior to discharge into the environment (receiving water). As dyes are generally stable to light, oxidizing agent and have poor biodegradability, removal of dyes from industrial effluents is considered as a challenging problem in the control of environmental pollution. Biological treatment, activated carbon adsorption, ion-exchange and chemical coagulation are some of the conventional treatment processes of dye removal, but all these still have their own disadvantages and limitations [4–7]. Though activated carbon has proven its efficiency and capability in removing various types of pollutants due its high porosity and large surface area (500–200 $m^2\ g^{-1}$), but widespread application is restricted due to high cost, difficult disposal and regeneration [8]. Therefore, research is intensified to search for new materials to serve as the potential alternative to dye removal from wastewater. Photocatalytic purification of wastewater using semiconductor nanomaterials such as ZnO, TiO_2, CuO, etc., has attracted tremendous interest nowadays because of their nontoxicity, high photocatalytic efficiency, high physical and chemical stabilities and cost-effectiveness. ZnO is a versatile *n*-type semiconductor with excellent chemical and thermal stabilities with wide band gap of 3.37 eV and high excitation binding energy of 60 meV at room temperature [9]. Hence, it is considered as one of the potential photocatalysts for the degradation of various pollutants in wastewater. The photocatalytic activity of ZnO can be augmented using nanosized ZnO in the form of various shapes as nanoparticles, nanorods, nanotubes, etc. As the reduction in size increases the surface area, thus, enhancing the photocatalytic activity of ZnO. A number of physical and chemical approaches are available to synthesize ZnO nanoparticles (ZnO NPs), for example, hydrothermal method [10], solvothermal method [11,12], microemulsion method [13], microwave method [14], thermal decomposition [15], precipitation [16], sol–gel [17], laser ablation [18] and

sonochemical method [19]. Although these physical/chemical methods are effective to synthesize of ZnO NPs with different sizes and morphologies, but these methods are complex, and utilize hazardous organic solvents, toxic reagents, non-biodegradable stabilizing agents and expensive instruments along with the tedious process control. Therefore, there is great demand for developing a simple, safe and eco-friendly method for synthesizing ZnO NPs.

Biological synthesis of nanoparticles using plant extracts is becoming an emerging area of research in nano-biotechnology due to its simplicity, low cost, nontoxicity and environmentally friendly nature. Moreover, nanoparticles are produced by plant extracts are more stable and biocompatible in comparison with those produced by physical/chemical methods. Based on the literature, biosynthesis of ZnO NPs were reported by using plant extracts including *Aloe vera* (leaf) [20], *Nephelium lappaceum* L. (fruit peel) [21], *Corymbia citriodora* (leaf) [22], *Polygala tenuifolia* (root) [23], *Trifolium pratense* (flower) [24], *Rosa canina* (fruit) [25], *Zingiber officinale* (rhizome) [26], *Eucalyptus globulus* (leaf) [27] and *Vitex trifolia* L. (leaf) [28]. In the present work, we describe a green synthetic strategy to prepare ZnO NPs from *Garcinia mangostana* fruit pericarp extract. *Garcinia mangostana* L. (*G. mangostana*) is commonly known as mangosteen, and belongs to the family of Guttiferae. It can grow up to 6–25 m in height and is mainly found in Southeast Asian countries such as Indonesia, Malaysia, Vietnam, Thailand, Philippines and Sri Lanka. Mangosteen has dark purple to red-purple fruits. The edible portion of fruit (aril) is white, soft with a slightly sour taste and a pleasant aroma. It is the most economical and popularly consumed tropical fruits in the Southeast Asian countries. Consequently, large amounts of mangosteen pericarp (6–10 mm in thickness) are discarded as waste domestically. There are few applications of these pericarps were reported in the literature, for example, the pericarp was used in folk medicine in treatment of several human illnesses, including skin and wound infections, hemorrhoids, arthritis, tuberculosis, inflammation, genitourinary tract infections, fever and amoebic dysentery [29], and as biosorbents to remove toxic metals of Pb(II), Cd(II) and Co(II) from aqueous solution [30]. Another application includes their use as an effectual component as a sensitizer to fabricate dye-sensitized solar cells [31].

Herein, we demonstrate a green and eco-friendly route for the synthesis of ZnO NPs using aqueous extract of *G. mangostana* fruit pericarp. X-ray diffraction (XRD), energy dispersive X-ray spectroscopy (EDX), field emission scanning electron microscope (FESEM), transmission electron microscopy (TEM), Fourier transform infrared spectroscopy (FTIR) and UV–Vis spectroscopy were used for characterizing the biosynthesized ZnO NPs. The photocatalyst activity of biosynthesized ZnO NPs was also investigated using malachite green (MG) dye as the model pollutant under solar irradiation.

2. Experimental

2.1 *Materials*

G. mangostana fruits were purchased from a local market Kampar, Malaysia. Zinc nitrate hexahydrate ($Zn(NO_3)_2 \cdot 6H_2O$) and MG dye were purchased from Sigma-Aldrich, USA, and used as received. All aqueous solutions were prepared using distilled water. All glassware used was cleaned and washed with distilled water and dried before use.

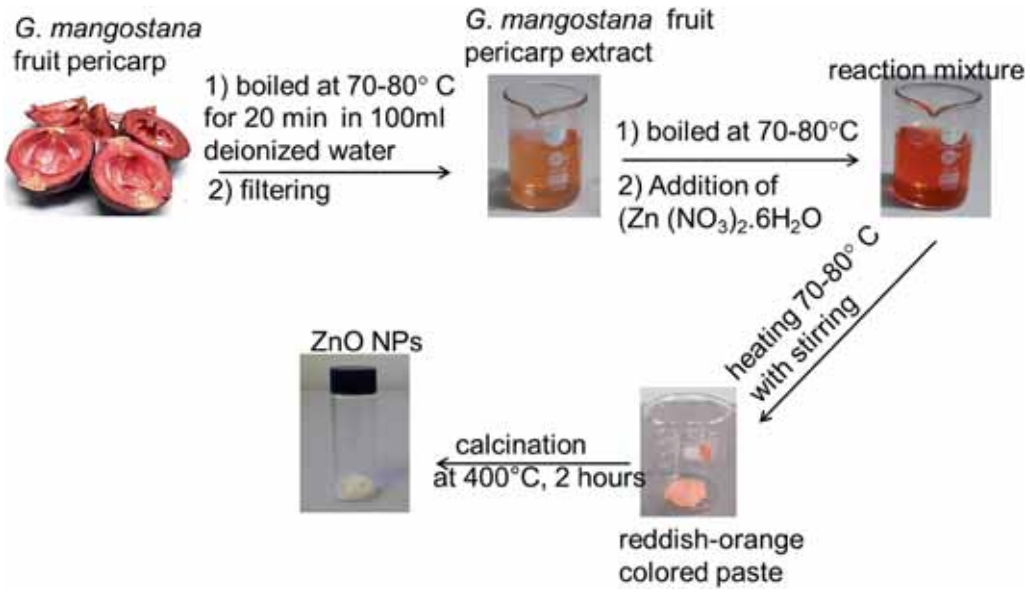

Scheme 1. Steps involved in biosynthesizing of ZnO NPs using aqueous extract of *Garcinia mangostana* fruit pericarp.

2.2 *Preparation of aqueous extract of G. mangostana fruit pericarp*

The fresh pericarps were washed thoroughly with distilled water to remove dust and organic impurities. About 8 g of pericarps were taken in a 250 ml beaker containing 100 ml deionized water and then, the pericarps were boiled at 70–80°C for 20 min. During the procedure of boiling, a pale brown coloured solution was formed and which was cooled at room temperature. Then, the extract was filtered with filter paper (Whatman no. 1) twice and filtrate was collected in a 100 ml beaker. This extract was then directly used in the synthesis of ZnO NPs.

2.3 *Synthesis of ZnO NPs*

Scheme 1 represents the synthesis of ZnO NPs using aqueous extract of *G. mangostana* fruit pericarp. To synthesize ZnO NPs, freshly prepared 50 ml *G. mangostana* fruit pericarp extract was taken in 100 ml beaker and boiled at 70–80°C. Later, about 4 g of zinc nitrate hexahydrate ($Zn(NO_3)_2 \cdot 6H_2O$) was added slowly into the hot pericarp extract and immediately reddish-brown coloured solution was formed. This reaction mixture was heated at 70–80°C with magnetic stirring. As the reaction progressed, the colour of the reaction solution slowly changed from reddish-brown to pale yellow and heating continued until the formation of reddish-orange coloured paste. The paste was then transferred to a ceramic crucible followed by heating in a furnace at 400°C for 2 h. The obtained pale white coloured powder was used for further studies.

2.4 *Characterization*

The crystal phase information of the sample was characterized from 10 to 80° in 2θ by an X-ray diffractometer with CuK α radiation (Shimadzu XRD 6000, Japan). Surface morphology of ZnO NPs was characterized by FESEM (JEOL JSM-6701F combined with EDX, Japan) and high resolution transmission electron microscope (HRTEM) (JEOL JEM 3010). UV–Vis absorption spectra were recorded by a UV–visible spectrophotometer (Perkin Elmer Lambda 35). The FTIR spectra of biosynthesized ZnO NPs were recorded by KBr pellet method using FTIR spectrophotometer (Perkin Elmer RX1).

2.5 *Photocatalytic activity of ZnO NPs*

The photocatalytic activity of the biologically synthesized ZnO NPs was evaluated by the degradation of an organic dye, MG under direct sunlight. In a typical process, 50 mg ZnO NPs were added into a beaker containing MG dye solution (50 ml, 10 mg l^{-1}). Prior to exposure to sunlight, the suspension was magnetically stirred in the dark for 30 min to reach the adsorption–desorption equilibrium. The photodegradation of MG dye was carried out on a sunny day between 11 am and 2 pm when there were minimum fluctuations in solar intensity. The experiment was carried out in UTAR, Kampar campus in the month of February (outside temperature

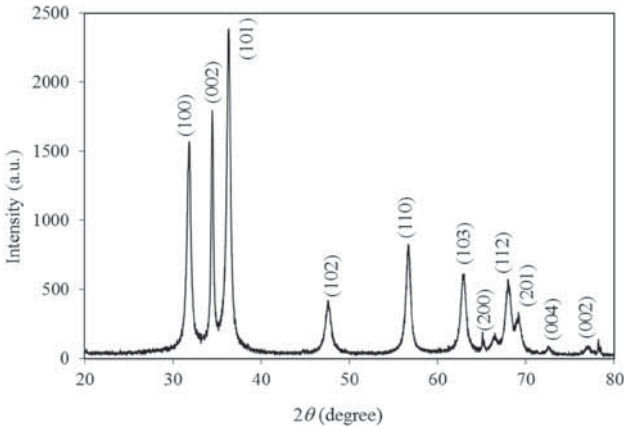

Figure 1. XRD pattern of biosynthesized ZnO NPs using *G. mangostana* fruit pericarp extract.

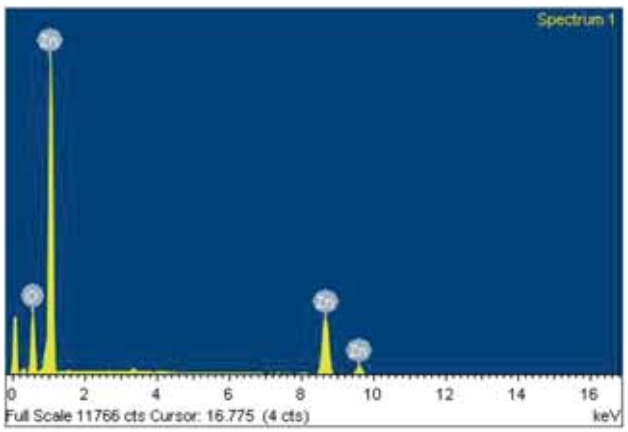

Figure 2. EDX spectrum of biosynthesized ZnO NPs.

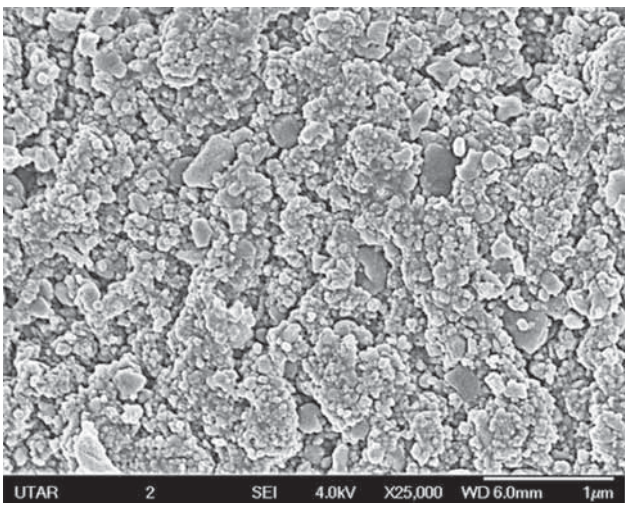

Figure 3. FESEM image of green-synthesized ZnO NPs.

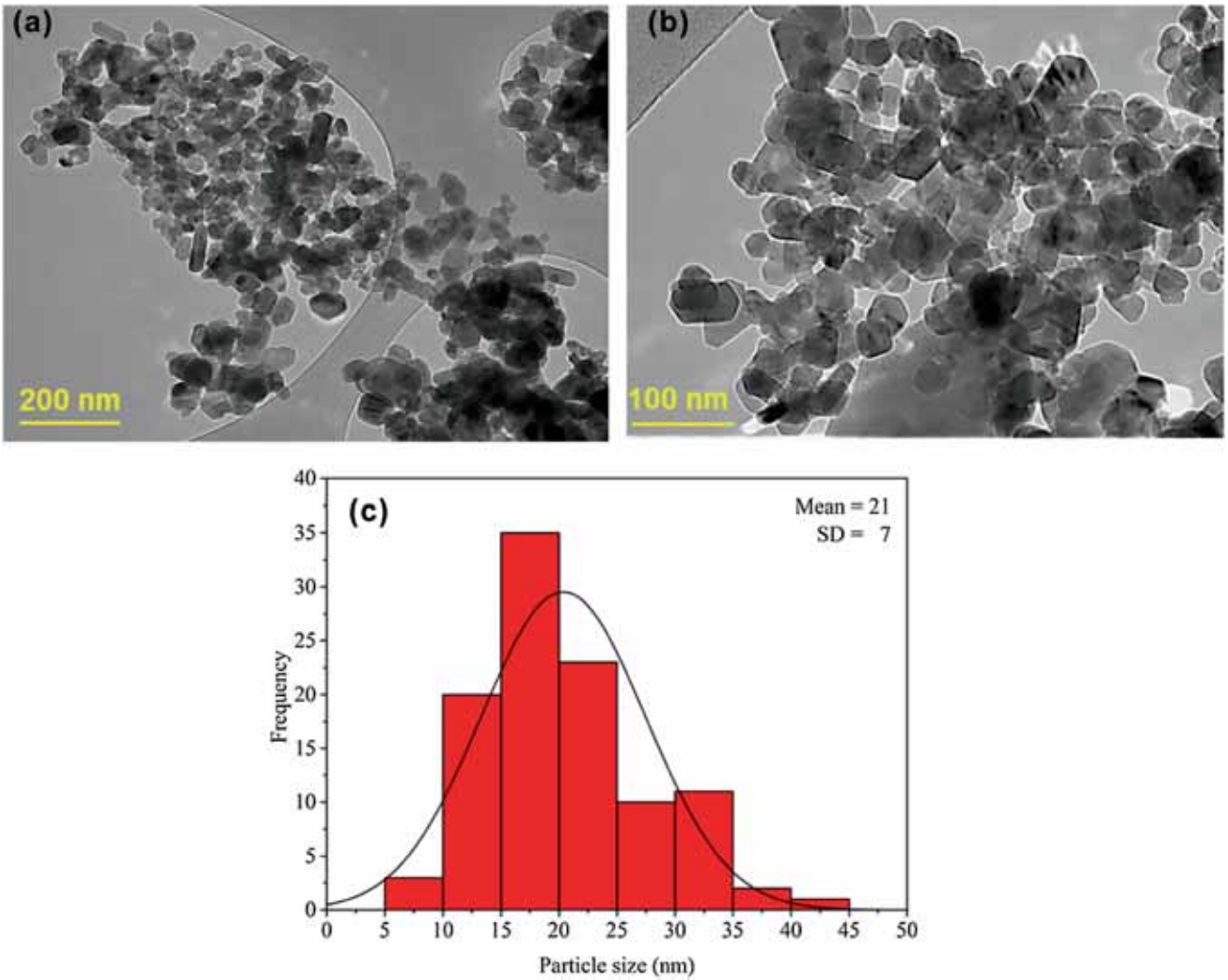

Figure 4. TEM images of ZnO NPs forms using *G. mangostana* fruit pericarp extract and histogram of particles size distribution of ZnO NPs.

was 30–35°C) on a sunny day when the average solar radiation was 4.35 kwh m^{-2} d^{-1}. At given time intervals, 10 ml of suspension was sampled and centrifuged (7000 rpm) for 10 min, the supernatant was collected for absorption analysis on a UV–Vis spectrophotometer. The absorbance of MG at 615 nm was used to measure the residual dye concentration. The degradation efficiency (%) was calculated using the below mentioned equation:

$$\text{Degradation efficiency (\%)} = \frac{C_o - C}{C_o} \times 100, \qquad (1)$$

where C_o is the initial concentration of MG dye solution (mg l^{-1}) and C the concentration of the MG dye solution (mg l^{-1}) after a certain irradiation time.

Moreover, possible intermediates formation during photocatalytic degradation of MG dye were determined by liquid chromatography-mass spectrophotometry (LC-MS) analysis

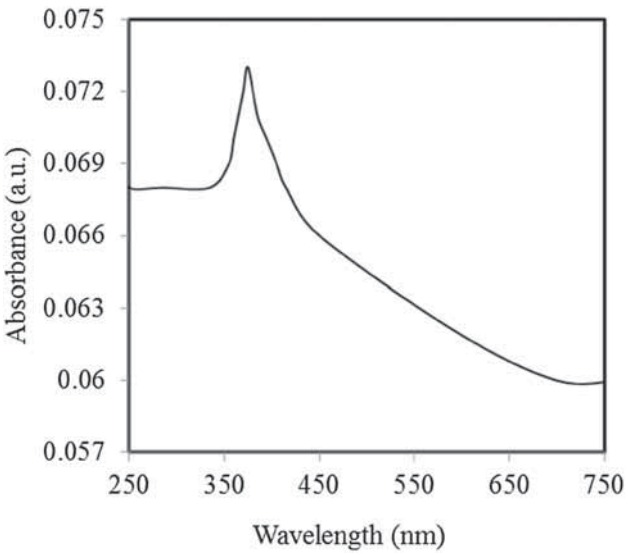

Figure 5. UV–Vis spectrum of biosynthesized ZnO NPs.

of degraded dye solution taken at different time intervals using an Agilent 6520 Accurate-Mass Q-TOF LC/MS (Agilent, USA) instrument. The mobile phase was a mixture of water (A) and acetonitrile (B) at 0.6 ml min^{-1} of the flow rate, and the gradient was set as follows: $t = 0$ min, A:B = 5:95 (V/V); $t = 30$ min, A:B = 95:5 (V/V). The column temperature was 30°C and injection volume was 20.00 µl using autosampler. The mass fragments to monitor were from 40 to 400 *m/z*.

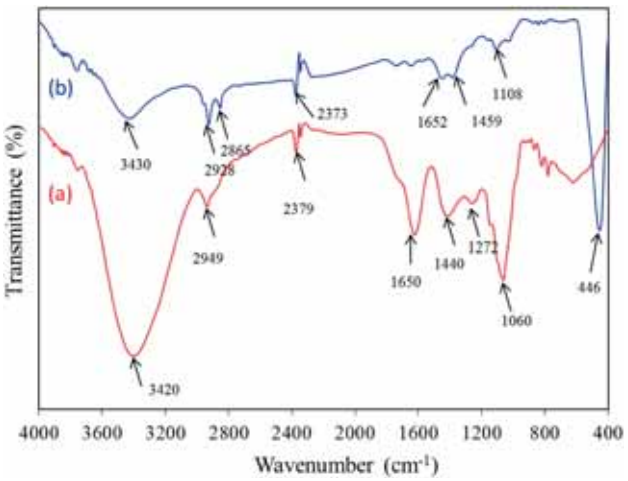

Figure 6. FTIR spectra of (**a**) pure *G. mangostana* fruit pericarp extract and (**b**) biosynthesized ZnO NPs by using *G. mangostana* fruit pericarp extract.

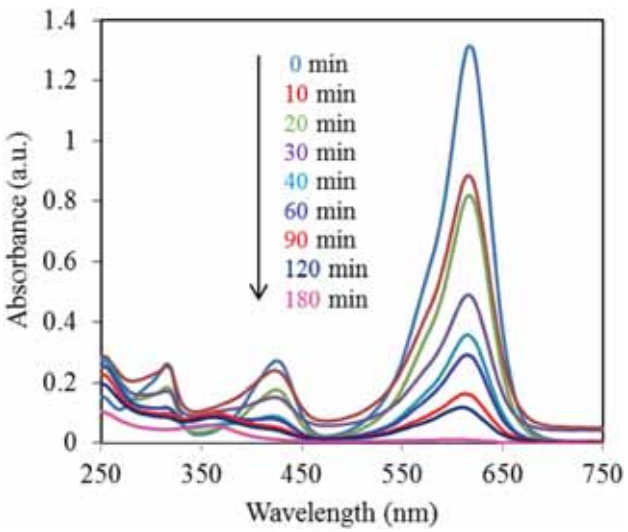

Figure 7. Time-dependent UV–Vis absorption spectra of photocatalytic degradation of MG dye in the presence of biosynthesized ZnO NPs.

3. Results and discussion

3.1 *Characterization of green synthesized ZnO NPs*

XRD technique was used to examine the crystal phases and crystallinity of the synthesized ZnO NPs. Figure 1 represents the XRD pattern of biosynthesized ZnO NPs. The distinct diffraction peaks at $2\theta = 31.81$, 34.44, 36.24, 47.52, 56.64, 62.82, 65.12, 66.32, 67.98, 69.14, 72.56 and 77.14° were assigned to (100), (002), (101), (102), (110), (103), (200), (112), (201) (004) and (002) planes, respectively. In figure 1, all the diffraction peaks were well indexed to the hexagonal phase (wurtzite structure) of ZnO, which are very close to standard values (JCPDS no. 36-1451). Similar XRD results were also observed in the reported literature for ZnO nanomaterials [32,33]. Interestingly, no reflection related with any impurity was detected in the pattern, up to the detection limit of XRD diffractometer, which further reveals that the prepared nanoparticles are pure ZnO. Moreover, the obtained diffraction reflections are well-defined with high intensity, which clearly confirmed that the biosynthesized ZnO NPs are well-crystalline. The crystallite size (D) of the biosynthesized ZnO NPs was calculated by Debye–Scherrer's equation i.e.,

$$D = \frac{0.94\lambda}{\beta\cos\theta}, \tag{2}$$

where λ is the wavelength (CuK α), β the full-width half-maximum (FWHM) and θ the diffraction angle. The average crystallite size was found to be 23.56 nm. The elemental information of the biosynthesized ZnO NPs was analysed by EDX. As shown in figure 2, the spectrum of the sample presents only the existence of zinc (Zn) and oxygen (O). No other peak related with any other impurity was detected in the spectrum suggesting the high purity of formed ZnO NPs. Moreover, the weight percentage of zinc and oxygen was calculated to be 71.9 and 28.1%, respectively, which is in agreement with

Figure 8. Photograph shows gradual change in MG dye colour from bluish-green to colourless by solar irradiation.

those previously reported [34,35]. FESEM image of biosynthesized ZnO NPs is presented in figure 3 revealing that ZnO NPs with nearly spherical morphology and are agglomerated as a result of polarity and electrostatic attraction of nanoparticles. The size, shape and morphology of the green synthesized ZnO NPs were also investigated using TEM, which is represented by figure 4. TEM images indicate the shape of ZnO NPs are mostly spherical and some hexagonal shape particles are also seen in the micrograph. Figure 4c displays the histogram of the distribution of the particle size of ZnO NPs showing that typical sizes of the ZnO NPs are in the range between 5 and 45 nm and the average mean size was 21 nm, which is quite similar to the value obtained from XRD measurement.

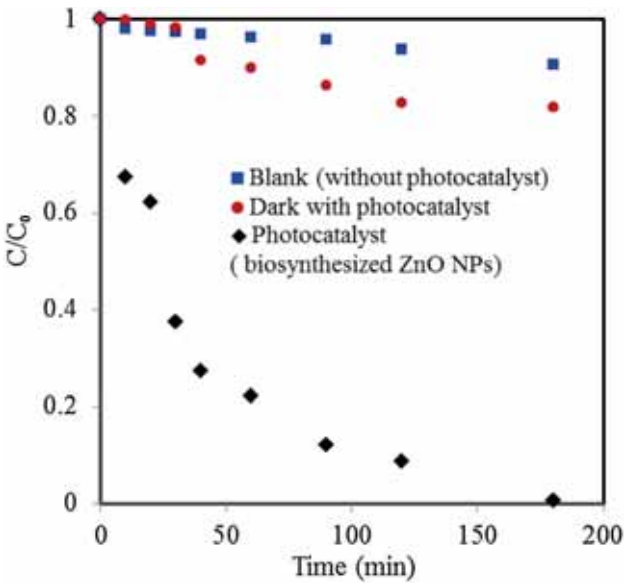

Figure 9. Degradation of MG dye solution as a function of different time intervals.

The room temperature UV–Vis absorption spectrum of the biosynthesized ZnO NPs is shown in figure 5. The ZnO NPs were dispersed in water with a concentration of 0.1 wt% and the solution was used to perform the UV–Vis measurement. The spectrum reveals a characteristic absorption peak at wavelength of 375 nm which can be assigned to the intrinsic band-gap absorption of ZnO due to the electron transitions from the valence band to conduction band ($O_{2p} \rightarrow Zn_{3d}$). The band gap energy ($E_g$) of the ZnO NP is calculated using the following equation:

$$E_g = hc/\lambda, \tag{3}$$

where h is the Planck's constant (6.662×10^{-34} Js), c the velocity of light (3×10^8 m s^{-1}) and λ (375 nm) the wavelength. The band gap energy for the ZnO NPs was found to be 3.32 eV.

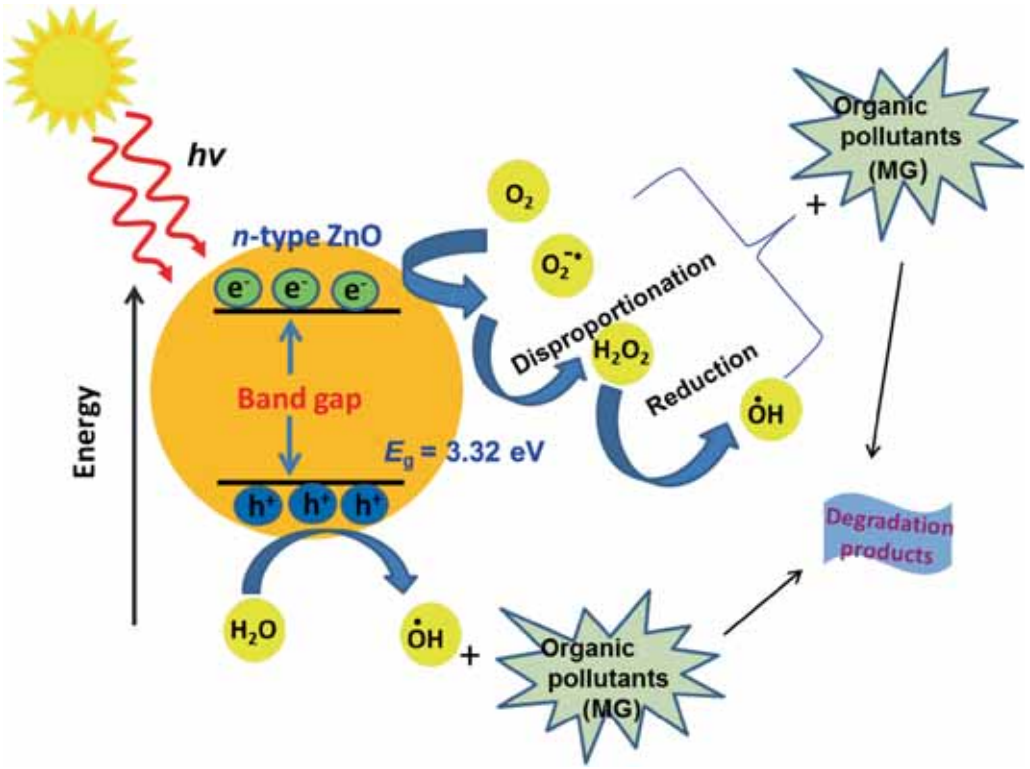

Scheme 2. Photocatalytic reaction mechanism of biosynthesized ZnO NPs.

ZnO NPs (3.32 eV) show blue shift compared to bulk ZnO (3.37 eV) and this observed blue shift may be due to the size effect [36].

FTIR was carried out to determine the potential functional groups of biomolecules that are responsible for the formation of ZnO NPs. Figure 6 shows the spectra obtained from pure *G. mangostana* pericarp extract and ZnO NPs synthesized using *G. mangostana* pericarp extract. The absorption bands at 3420 and 2949 cm^{-1} indicate the presence of O–H and C–H stretchings. The absorption peak is located at around 1650 cm^{-1} represents C=O stretching. The bands at 1440 and 1272 cm^{-1} are associated with the C–C stretch (in ring) of the aromatic group and C–OH vibrations of polyols. Finally, the absorption peak at 1060 cm^{-1} is attributed to C–O–C stretch. All the above results indicate phenol, flavonoid, xenthone and anthocyanin compounds are abundant in pericarp of *G. mangostana* [37]. On the other hand, the FTIR spectra of biosynthesized ZnO NPs have shown a sharp and intense absorption peak at 446 cm^{-1} confirming the stretching vibration of Zn–O [21] and very weak absorption bands at 3430,

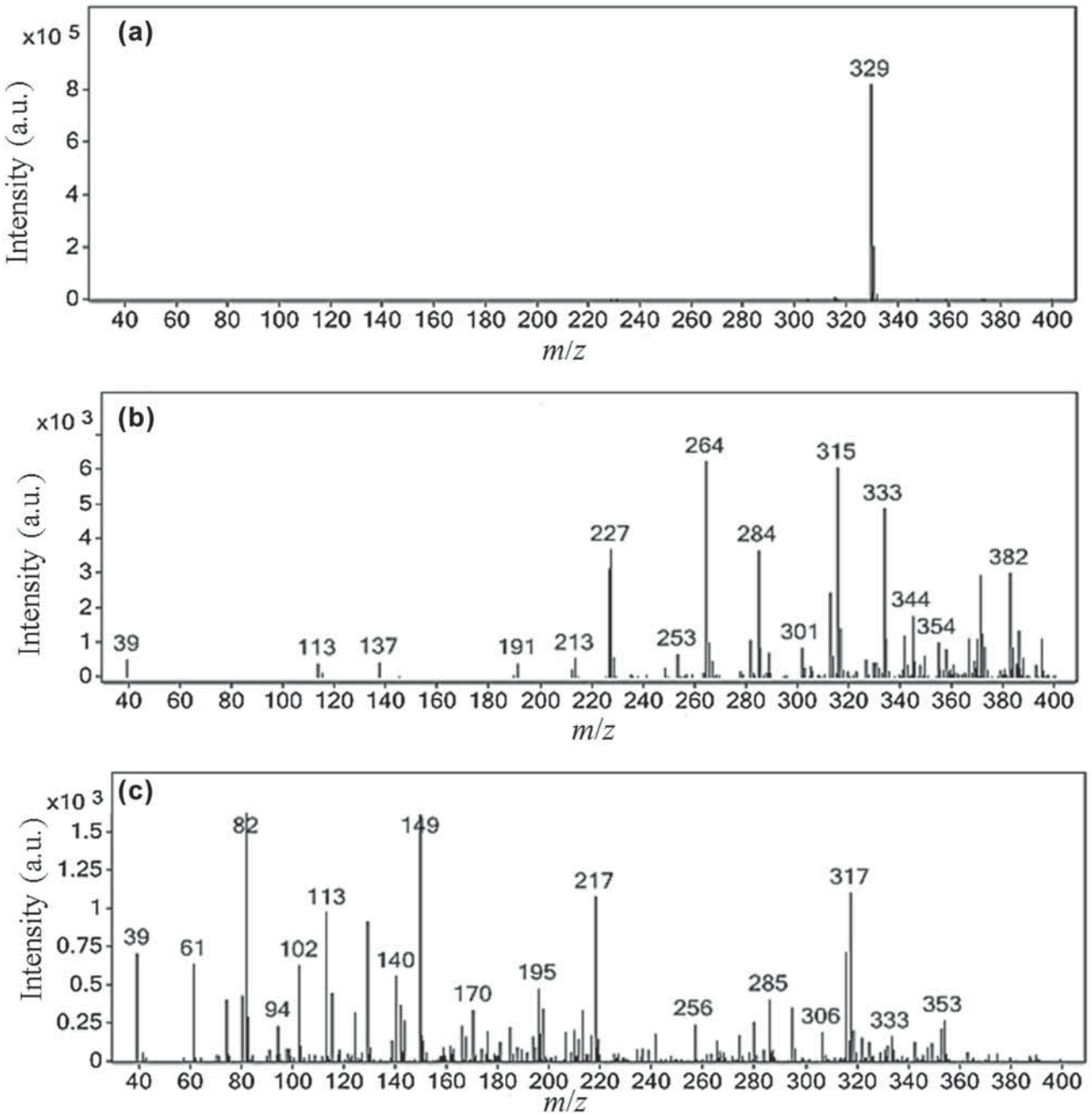

Figure 10. Mass spectra of (**a**) MG dye solution before solar irradiation and (**b**, **c**) after solar irradiation in the presence of ZnO NPs for 30 and 90 min, respectively.

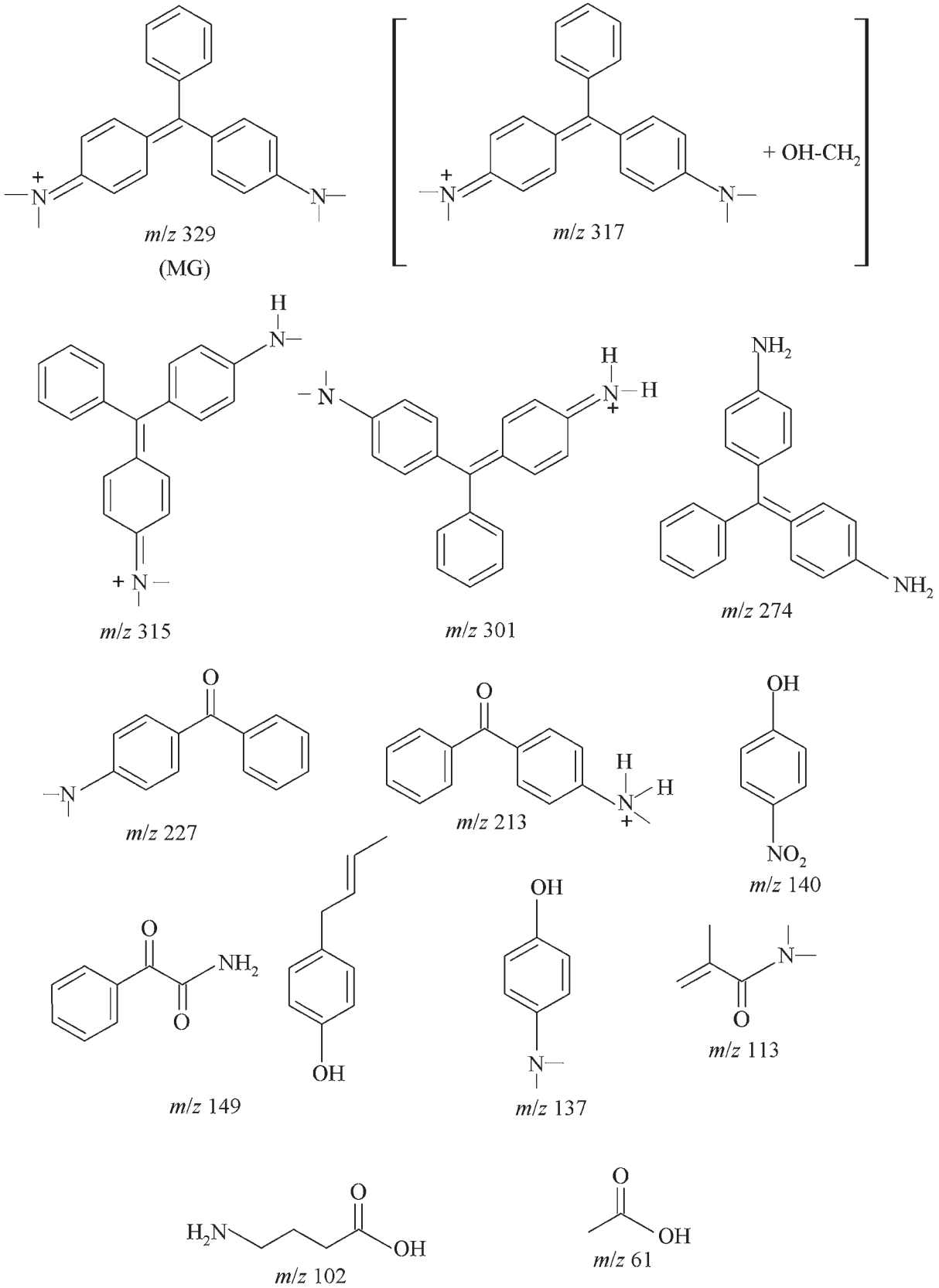

Figure 11. MG and its possible degradation products as analysed by LC-MS.

2928, 2865, 2373, 1652, 1459 and 1108 cm^{-1}, respectively. The shift observed in FTIR spectra of ZnO NPs after bioreduction bands such as 3420–3430, 2949–2982, 1637–1652, 1440–1445 and 1106–1108 cm^{-1} indicate the participation of phenols, flavonoids, xenthones, anthocyanin, etc. with functional groups OH, C=O, COOH, C–O–C, etc. in bioreduction reactions.

3.2 *Investigation of photocatalytic activity of biosynthesized ZnO NPs by degradation of MG dye under solar irradiation*

The photocatalytic activity of biosynthesized ZnO NPs was investigated by the degradation of MG dye in aqueous solution under sunlight irradiation. MG is a cationic triphenylmethane dye, and is one of the largest groups of hazardous dyes. It is commonly utilized in aquaculture industry as an effective fungicide [38], in textile industry as a colouring agent [39] and in industries of leather, paper and pharmaceutical, owing to its low price, readily availability and high efficiency [40]. Figure 7 shows the changes in the MG absorption spectra during photocatalytic degradation with ZnO nanophotocatalyst at different solar irradiation times varying from 0 to 180 min. About 99% of MG was degraded within 180 min of irradiation. Photodegradation of MG was also visually detected by gradual change in colour of the dye solution from bluish-green to colourless (figure 8). The results show that MG dye with the strong absorption maxima at 615 nm due to the chromophoric group and it was getting diminished gradually with the increase in irradiation time and become invisible within 180 min of irradiation indicating that the chromophore in MG molecules was completely removed. It is also interesting to notice that a hypsochromic shift occurred simultaneously with increasing irradiation time and the maximum absorption wavelength shifts from 615 to 605 nm. The hypsochromic shift is caused by an *N*-demethylation process [41]. The absorbance peaks at 425 and 315 nm were obviously disappeared under solar irradiation, which indicates that the entire conjugated structure of MG was destroyed. Notably, there is a new weak absorbance peak appeared at 355 nm after 90 min, which is possibly caused by benzene ring opening and cleavage of the central carbon.

The ratios of the concentration of dye, C to the initial concentration, C_o of the dye (C/C_o) at different times of sun light exposure, were plotted against the time of sun light exposure to compare the efficiency of the degradation under various experimental conditions as shown in figure 9. It was noticed that only 6.25% degradation of MG dye was found when irradiated under natural sunlight in the absence of biosynthesized ZnO NPs, which is due to photolysis of MG. For the same MG dye solution, the degradation efficiency with biosynthesized ZnO NPs in the dark for 180 min was only 13.72%, which can be attributed to the adsorption of MG on ZnO NPs. On the other hand, when the MG dye solution was exposed to the sunlight for 180 min in the presence of the biosynthesized ZnO NPs, the degradation efficiency of MG dye was almost 99% because of efficient oxidation through hydroxyl radicals (•OH) produced from the photocatalytic reaction. The detailed mechanism is shown in scheme 2. ZnO NPs successfully degraded MG dye into less harmful end products like CO_2, H_2O, NO_2, NO, etc.

MG and the degradation products formed during the photodegradation process in the presence of ZnO NPs under solar irradiation were analysed by LC-MS and identified by interpretation of their mass spectra data presenting their molecule ion peaks with respect to m/z (where m is molecular weight of the intermediates in the mass spectra). Figure 10a represents the MS spectrum of MG dye in aqueous solution before irradiation and figure 10b and c represents the MS spectra of MG dye in aqueous solution after solar irradiation for 30 and 90 min, respectively, with ZnO nanophotocatalyst. The parent molecular ion peak of MG at 329 m/z was detected before solar irradiation of the MG dye solution (figure 10a). However, after solar irradiation (for 30 and 90 min, figure 10 b and c) the m/z at 329 was split into various mass (m/z) signals due to photodegradation of MG dye molecules in the presence ZnO photocatalyst. The possible degradation species detected by LC-MS from MG dye solution using biosynthesized ZnO NPs at different solar irradiation times are shown in figure 11.

The reaction kinetics of photocatalytic degradation of MG dye using biosynthesized ZnO NPs are also investigated using Langmuir–Hinshelwood kinetic model [42], whose equation is written below:

$$\ln(C_o/C) = kt, \tag{4}$$

where C_o and C are the concentration of MG dye solutions before and after solar irradiation, k is the apparent rate constant which is obtained from the slope and t the time duration of the photocatalytic reaction. Figure 12 displays

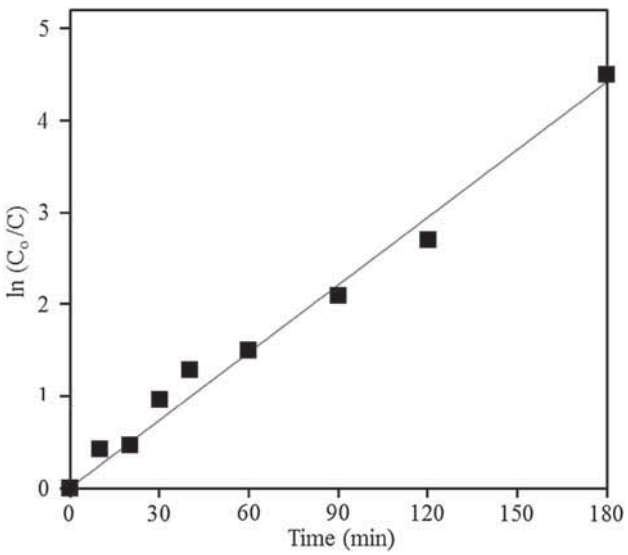

Figure 12. Plot of ln (C_o/C) *vs.* time, displaying the photocatalytic degradation of MG dye.

the plot of $\ln(C_o/C)$ *vs.* time. According to the equation, it was observed that the photocatalytic degradation of MG dye followed pseudo-first-order kinetics and the value of k was found to be 0.0245 min^{-1}.

4. Conclusions

In conclusion, we have developed an economically and environmentally benign, efficient and safe procedure for the green synthesis of ZnO NPs using *G. mangostana* fruit pericarp extract without use of toxic and hazardous materials. The detailed characterization results revealed that biosynthesised ZnO NPs are well-crystalline, possessing hexagonal wurtzite phase with an average size of 21 nm and exhibiting good optical properties. The photocatalytic activity of biosynthesized ZnO NPs was evaluated by the photodegradation of MG dye. The results indicate that the biosynthesized ZnO NPs have shown an excellent photocatalytic performance by almost complete degradation of MG dye on exposure to natural sunlight. Thus, biosynthesized ZnO NPs were proved as an effective photocatalyst, which can efficiently be utilized for the degradation of harmful and toxic pollutants persisting in aquatic environment.

Acknowledgements

We would like to thank Universiti Tunku Abdul Rahman (UTAR) for financial support and also providing all necessary facilities to carry out this research work successfully.

References

[1] Anirudhan T S, Suchithra P S and Radhakrishnan P G 2009 *Appl. Clay Sci.* **43** 336
[2] Nassar M Y, Ahmed I S, Mohamed T Y and Khatab M 2016 *RSC Adv.* **6** 20001
[3] Mittal A, Mittal J, Kurup L and Singh A 2006 *J. Hazard. Mater.* **138** 95
[4] Xu X, Gao B Y, Yue Q Y and Zhong Q Q 2010 *J. Hazard. Mater.* **182** 1
[5] Sarayu K and Sandhya S 2012 *Appl. Biochem. Biotechnol.* **167** 645
[6] Yagub M T, Sen T K, Afroze S and Ang H M 2014 *Adv. Colloid Interface Sci.* **209** 172
[7] Verma A K, Dash R R and Bhunia P 2012 *J. Environ. Manage.* **93** 154
[8] Malik P K 2002 *Dyes Pigment* **56** 239
[9] Özgüra Ü, Alivov Ya I, Liu C, Tekeb A, Reshchikov M A, Doğanc S *et al* 2005 *Appl. Phys.* **98** 041301
[10] Bharti D B and Bharati A V 2017 *Luminescence* **32** 317
[11] Anžlovar A, Marinšek M, Orel Z C and Žigon M 2015 *Mater. Des.* **86** 347
[12] Ghoshal T, Biswas S, Paul M and De S K 2009 *J. Nanosci. Nanotechnol.* **9** 5973
[13] Talebiana N, Amininezhada S M and Doudib M 2013 *J. Photochem. Photobiol. B* **120** 66
[14] Promnopas W, Thongtem T and Thongtem S 2015 *Superlattices Microstruct.* **78** 71
[15] Kumar S S, Venkateswarlu P, Rao V R and Rao G N *Int. Nano Lett.* **3** 1
[16] Moharram A H, Mansour S A, Hussein M A and Rashad M 2014 *J. Nanomater.* **2014** 1
[17] Omria K, Najeha I, Dhahria R, El Ghoula J and El Mira L 2014 *Microelectron. Eng.* **128** 53
[18] Jajarmi R, Zakaria A, Ahangar H A, Darroudi M, Zak A K and Drummen G P C 2012 *J. Alloys Compd.* **516** 41
[19] Yadav R S, Mishra P and Pandey A C 2008 *Ultrason. Sonochem.* **15** 863
[20] Ali K, Dwivedi S, Azam A, Saquib Q, Al-Said M S, Alkhedhairy A A *et al* 2016 *J. Colloid Interface Sci.* **472** 145
[21] Karnan T and Selvakumar S A S 2016 *J. Mol. Struct.* **1125** 358
[22] Zheng Y, Fu L, Han F, Wang A, Cai W, Yu J *et al* 2015 *Green Chem. Lett. Rev.* **8** 59
[23] Nagajyothi P C, Ju S, Jun I, Sreekanth T V M, Joong K and Mook H 2015 *J. Photochem. Photobiol. B* **146** 10
[24] Dobrucka R and Długaszewska J 2016 *Saudi J. Biol. Sci.* **23** 517
[25] Jafarirad S, Mehrabi M, Divband B and Kosari-Nasab M 2016 *Mater. Sci. Eng. C* **59** 296
[26] Anbuvannan M, Ramesh M, Viruthagiri G, Shanmugam N and Kannadasan N 2015 *Spectrochim. Acta: Part A* **143** 304
[27] Balaji S and Kumar M B 2017 *Adv. Powder Technol.* **28** 785
[28] Elumalai K, Velmurugan S, Ravi S, Kathiravan V and Raj G A 2015 *Adv. Powder Technol.* **26** 1639
[29] Pedraza-Chaverri J, Cárdenas-Rodríguez N, Orozco-Ibarra M and Pérez-Rojas J M 2008 *Food Chem. Toxicol.* **46** 3227
[30] Zein R, Suhaili R, Earnestly F, Indrawati and Munaf E 2010 *J. Hazard. Mater.* **181** 52
[31] Zhou H, Wu L, Gao Y and Ma T 2011 *J. Photochem. Photobiol. A Chem.* **219** 188
[32] Umar A, Chauhan M S, Chauhan S, Kumar R, Kumar S, Al-Sayari S A *et al* 2011 *J. Colloid Interface Sci.* **363** 521
[33] Kumar R, Kumar G and Umar A 2013 *Mater. Lett.* **97** 100
[34] Salam H A, Sivaraj R and Venckatesh R 2014 *Mater. Lett.* **131** 16
[35] Chandrappa K G, Venkatesha T V, Vathsala K and Shivakumara C 2010 *J. Nanopart. Res.* **12** 2667
[36] Wang C, Shen E, Wang E, Gao L, Kang Z, Tian C *et al* 2005 *Mater. Lett.* **59** 2867
[37] Obolskiy D, Pischel I, Siriwatanametanon N and Heinrich M 2009 *Phytother. Res.* **23** 1047
[38] Rahman I A, Saad B, Shaidan S and Sya Rizal E S 2005 *Bioresour. Technol.* **96** 1578
[39] Ju Y, Yang S, Ding Y, Sun C, Zhang A and Wang L 2008 *J. Phys. Chem. A* **112** 11172
[40] Schnick R A 1988 *Prog. Fish-Cult.* **50** 190
[41] Behnajady M A, Modirshahla N, Shokri M and Vahid B 2008 *Ultrason. Sonochem.* **15** 1009
[42] Hou J, Wang Z, Jiao S and Zhu H J 2012 *Cryst. Eng. Commun.* **14** 5923